

We are IntechOpen, the world's leading publisher of Open Access books Built by scientists, for scientists

6,900

Open access books available

186,000

International authors and editors

200M

Downloads

Our authors are among the

154

Countries delivered to

TOP 1%

most cited scientists

12.2%

Contributors from top 500 universities



WEB OF SCIENCE™

Selection of our books indexed in the Book Citation Index
in Web of Science™ Core Collection (BKCI)

Interested in publishing with us?
Contact book.department@intechopen.com

Numbers displayed above are based on latest data collected.
For more information visit www.intechopen.com



Active and Passive Control of Flow Past a Cavity

Seiichiro Izawa
Tohoku University
Japan

1. Introduction

Flow past open cavities is well known to give rise to highly coherent and self-sustained oscillations, leading to undesirable aeroacoustic resonance. Cavity flows are encountered not only in engineering applications but also our daily life, for example, the weapon bays, landing gears and wheel wells of aircrafts, in the depressions of submarine and ship hulls, in the pantograph recess of high-speed train, in the sunroof of cars or in the closed side branches of pipelines. Periodic and intense aeroacoustic vibrations deriving from the self-sustained oscillations of cavity flows can give rise to structural fatigue, optical distortion and store separation problems, especially for high-speed aircrafts. For a typical open-cavity flow, the induced acoustic level exceeds 160dB at transonic Mach numbers (MacManus & Doran, 2008) and it still reaches approximately 130dB at around 100 ~110km/h for passenger vehicles because the passenger compartment acts as a Helmholtz resonator (Gloerfelt, 2009). Cavity-like geometries are also observed in places such as urban canyons, rivers and lakes. For these environmental fields, cavity flows affect the mass transfer processes of various pollutants and chemical toxic substances that occur between the cavity and the main flow (Chang et al., 2006). In the last decade, open cavities have attracted many researchers engaged in scramjet engines with regard to mixing and flame-holding enhancement for supersonic combustion (Asai & Nishioka, 2003; Kim et al., 2004). Because of these issues across a wide range of applications, cavity flows have been of practical and academic interests for more than a half-century.

The flow-induced oscillations in an open cavity arise from a feedback loop formed as a result of successive events that take place in sequence. Figure 1 illustrates the schematic of cavity flows with an acoustic resonance. A boundary layer of thickness δ separates at the upstream edge of the cavity of length L and depth D . The resulting separating shear layer is convectively unstable due to Kelvin-Helmholtz instability, and it soon rolls up into vortices. Every time the organized vortical structures collide the downstream corner, the expansion waves are radiated from the corner owing to the vorticity distortion at low Mach numbers (Yokoyama & Kato, 2009), while as Mach number increases, the compression waves are generated near the downstream corner, especially for supersonic flows (Nishioka et al., 2002). It should be noted that the hypersonic shear layers do not always roll up into isolated vortices, just forming wavy patterns. The strength of these induced waves is determined by the relative position of the traveling vortices and the downstream corner. Rockwell & Knisely (1978) classified the vortex-corner interactions into four possible events on the basis of flow visualizations: Complete Escape (CE), Partial Escape (PE), Partial Clipping (PC) and Complete Clipping (CP). The incident acoustic waves propagate inside the cavity towards the upstream corner and

determine the initial amplitude and phase of the instability waves in the separating shear layer through the receptivity process. In particular, when the process is coupled with an acoustic cavity resonance, intense aerodynamics tones are generated in and around the cavity at one or more resonant discrete frequencies. This mechanism is common to basically all cavity tones regardless of the Mach number, known as shear-layer mode or Rossiter mode (Rossiter, 1964). This type of aeroacoustic tones is referred as the cavity noise. According to Rossiter's empirical formula, the resonant frequencies are given by

$$\frac{fL}{U_\infty} = \frac{m - \alpha}{M + 1/\kappa} \quad (1)$$

where f is the frequency at a given mode number $m = 1, 2, 3, \dots$ and M is the freestream Mach number. The empirical constants α and κ correspond to the average convection speed of vortices traveling over the cavity normalized by freestream speed and the phase delay of vortices against the upstream traveling acoustic waves. For example, $\alpha = 0.25$ and $\kappa = 0.57$ are derived from the experiment under the condition that $L/D = 4$ and the Mach number range $M = 0.4 \sim 1.2$. These values are intrinsically dependent on the flow conditions and the aspect ratio of the cavity, L/D . Some modified formulas have been proposed in the past (e.g., Heller et al., 1971; Asai & Nishioka, 2003). In addition to experimental studies, a number of computational studies have been performed to predict the vibration and acoustics associated with cavity flows for various Mach numbers (e.g., Grace, 2001; Gloerfelt et al., 2003; Larchevêque et al., 2007; De Roeck et al., 2009). The noise generated by circular cavities, not rectangular cavities, was also investigated by Marsden et al. (2008) and Chicheportiche & Gloerfelt (2010).

Flow patterns over the cavity can be roughly categorized into two different types, depending on the aspect ratio L/D . As the cavity is elongated, a free shear layer eventually reattaches on the floor of the cavity before reaching the downstream wall. Once the reattachment occurs, one more recirculating region with opposite rotating direction appears near the downstream side. This type of cavities is called the "closed cavity". Closed cavity flows can be regarded as

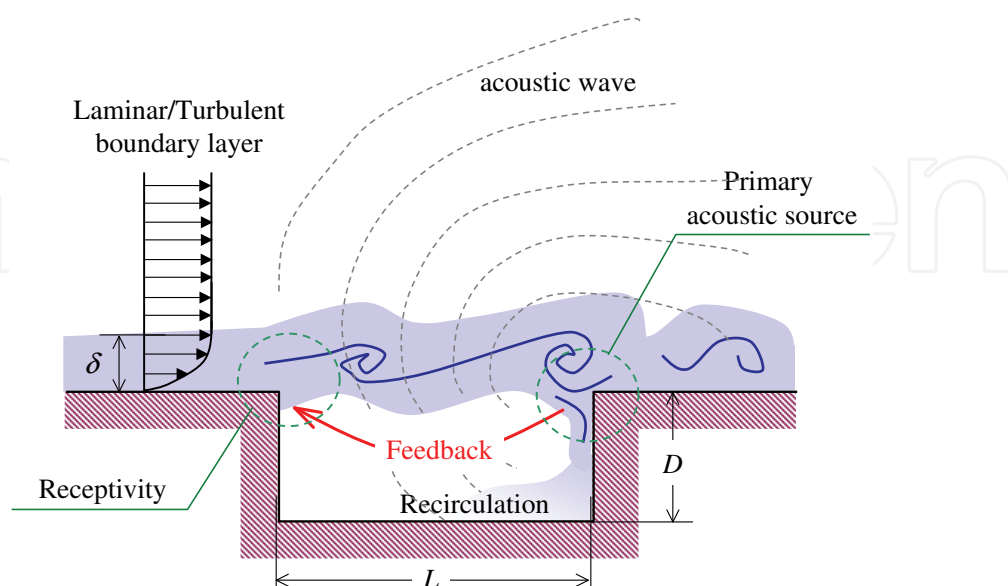


Fig. 1. Schematic of cavity flows.

the flow, which combines the backward-facing step with the forward-facing step. The cavities without reattachment are termed "open cavity". Between these two states, the cavity flows exhibit both characteristics, and are called the "transitional cavity". The open cavity flows are much more complex than the closed cavity flows, because the self-sustained oscillations only occurs in the upstream cavities. Flow visualizations have been presented to observe fluid motions inside the open cavity with different aspect ratios L/D (e.g., Faure et al., 2006).

A variety of control techniques for cavity resonance suppression have been tested over the years. These approaches can be classified into three types by the controlling locations: the leading edge, downstream edge, and the floor of the cavity. Most of the methods to control cavity flows tried to actively control the separating flow by introducing minute velocity fluctuations at the leading edge of a cavity, where the receptivity of the flow is most sensitive to the small disturbances. Raman et al. (1999) investigated the effect of miniaturized bi-stable fluidic oscillator on the cavity noise resonance, where its frequency and velocity depended on the supplied pressure. The fluidic device located at the upstream end of the cavity floor could suppress the cavity noise by 10db with mass injection rates of the order of 0.12% of the main flow, while it lost the effect near the downstream end of the cavity. Hémon et al. (2002) used piezoelectric bimorph elements as a flap-type actuator, which allows to generate a series of two-dimensional vortices forced at a different frequency from the natural resonance frequency. Kegerise et al. (2002) have tested the adaptive feedback controller together with the infinite-impulse filter response (IIR) filters to activate similar piezoelectric flaps. Rowley et al. (2003, 2005) injected the zero-net-mass airflows at the leading edge on the basis of pressure information at the wall inside the cavity. Huang & Zhang (2010) reported that the streamwise plasma actuators located on the upstream surface of the cavity was more effective than the spanwise actuators in cavity noise attenuation.

Besides the leading edge control, Micheau et al. (2005) used the vibrating surface that is an aluminum beam located along the downstream edge and attached to a shaker. They obtained significant cavity noise attenuation with an adjustable narrow-band controller using wall-mounted microphones placed at the bottom of the cavity. Yoshida et al. (2006) numerically investigated the effect of sliding floor of the cavity on the flow-induced cavity oscillations. The shear layer oscillations could be suppressed by creating stationary vortices inside the cavity, when the floor velocity was larger than 19% of the freestream velocity in the streamwise direction, or less than -10% . Detailed reviews of active control have been provided by Williams & Rowley (2006) and Cattafesta et al. (2008).

In addition to various active control techniques, passive control approaches have also been tested, though their numbers are smaller. For instance, MacManus & Doran (2008) added a backward-facing platform at the leading edge of the cavity against transonic Mach number flows, $M = 0.7 \sim 0.9$. They pointed out that a large recirculation bubble sitting on top of the step face might contribute to the noise attenuation. Kuo & Chang (1998) and Kuo & Huang (2003) discussed the effect of horizontal plate above the cavity on the oscillating flow structures within the cavity below. They (2001) also investigated the influence of sloped floor or fence on the flat floor of the cavity, focusing on the recirculating flow inside the cavity.

On the other hand, our wind tunnel experiments for cavity flows were conducted at low Mach numbers. The present work reviews a series of our studies to control cavity flows actively and passively, discussing their noise suppression mechanism. As an active control device, we use an array of piezoelectric actuators, oscillating vortex generators (VG), synthetic jets and fluidic oscillators. Synthetic jets, which are generated by a combination of loudspeaker and resonator, are ejected through open slots, while the intermittent jets are provided by the fluidic

oscillators. Vortex generators attached on the upstream surface are designed to introduce the streamwise vortices of alternate rotating directions into the shear layer. These devices are attached on the upstream wall of a cavity except for VG to add the weak periodic velocity fluctuations to the shear layer. Their operating frequency is chosen as the natural frequency of the shear layer. It should be noted that our method, quite different from any others, controls only the timing of the separation at the leading edge depending on the spanwise location. Therefore, the wavy patterns of velocity fluctuations side-by-side with 180 degrees phase difference are generated in the flow. As a result, the pressure fluctuations hence the sound waves coming out will also be 180 degrees out of phase, and then, these opposite-signed sound waves will eventually cancel each other faraway from the cavity though the noise generation at the source itself is not reduced. The competitive advantage of phase control is ascribed to low energy consumption compared with other methods, which changes the frequency of the oscillation or eliminates the oscillation itself. We have also performed the passive control experiments using a small thin plate inserted inside the shear layer and a small blockage set at the bottom of the cavity. The effect of the size and location of the obstacle on the noise suppression is investigated.

This paper consists of two main sections. The first section reviews our open-loop control of flow-induced cavity noise. In the second part, we describe the passive control experiments.

2. Experimental setup

Experiments were conducted in the small-scale low-turbulence wind tunnel at the Institute of Fluid Science (IFS) of Tohoku University. The wind tunnel is a closed circuit type and has an octagonal nozzle with a cross section dimensions 293mm from wall to wall, and 911mm-long open type test section. The freestream turbulence level at the test section was roughly 0.1 ~ 1.5% of freestream velocity U_∞ that is 18 ~ 30 m/s.

Figure 2 shows a rectangular cavity model used in the experiment. The model was slightly tilted raising the trailing edge to prevent flow separation near the leading edge. The cavity of streamwise length L and depth D was placed 300 ~ 450mm downstream from the leading edge. Beneath the flat plate surface, a resonator is used to simulate a deep cavity environment because the peaky noise is not generated in the shallow cavity case when the flow before separation is turbulent. The natural wavy pattern of velocity fluctuation in the cavity is two-dimensional so that two end plates are attached on both spanwise ends of the plate to maintain the flow conditions. The origin of coordinate system is at the center of the upstream edge of the cavity, where x , y , z -axes are in the streamwise, wall-normal, and spanwise directions.

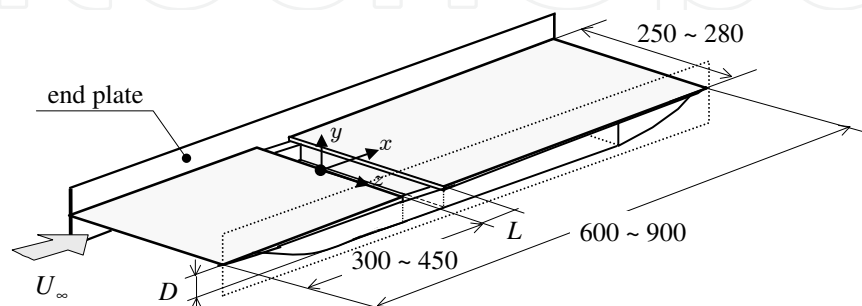


Fig. 2. Schematic of cavity model.

The velocity fields are mainly measured by a hot-wire probe on a three-dimensional traversing mechanism. The acoustic measurement are made using a 1/2-inch (1.27mm) condenser microphone from the location at 500 ~ 1,000mm above the center of the cavity, which is determined by the frequency of radiated cavity noise to ensure the far field. The signals from the hot-wire probe and microphone are digitized by a 16 bit (5kHz) A/D converter after passing an anti-alias filter, which has a 2.5kHz cut-off frequency. And then, the data are stored and processed by a computer running on a Linux operating system.

3. Active control

Open-loop control of cavity flows has been performed using various type actuators: an array of piezoelectric actuators, oscillating vortex generators, synthetic jets and fluidic oscillators. In the following sections, we describe the control effects of each actuator on the cavity noise attenuation.

3.1 Piezoelectric actuator

Some certain materials can acquire a charge in response to mechanical strain, and vice versa, they become lengthened or shortened if they are exposed to an electric field. This characteristic is known as piezoelectricity. Lead zirconate titanate ($\text{Pb}[\text{Zr}_x, \text{Ti}_{1-x}]\text{O}_3$, $0 < x < 1$), called PZT, is a popular material that shows the piezoelectric effect. PZT is deformed by approximately 0.1% of the static dimension when an external electric field is applied. We use two types of PZT ceramic elements (FUJI CERAMICS CORPORATION), unimorph and bimorph, as an actuator (Yokokawa et al., 2000, 2001; Fukunishi et al., 2002). A bimorph element consists of two unimorph elements so as to produce large displacement, because electric field causes one element to extend and the other element to contract. The dimensions of one PZT ceramic element used in our experiments are 50mm long, 60mm wide and 0.3mm thick for unimorph type, and 25mm long, 30mm wide and 0.5mm thick for bimorph type. Four unimorph and eight bimorph actuator pieces are installed at the leading edge of the cavity of length $L = 50\text{mm}$, depth $D = 27.5\text{mm}$ and width $W = 250\text{mm}$ respectively, as shown in Fig. 3. Since the upstream side or lower side of these actuators are glued onto the wall, streamwise displacement can be obtained by expanding and contracting motions for unimorph type and bending motion for bimorph type. It should be noted that the maximum displacements are several micrometers for unimorph type and approximately tenfold increase in bimorph type, when $70V_{\text{rms}}$ is applied to the actuators. Thus, a thin plastic plate of 0.2mm thick is inserted between the upstream sidewall and each bimorph actuator to prevent unfavorable noise generation caused by the actuator hitting the solid wall.

Each actuator is wired separately so as to operate them independently. The sinusoidal operating signals of voltage are generated by a frequency synthesizer (TOA FS-1301) and amplified by a high-speed voltage amplifier (NF ELECTRONIC INSTRUMENTS 4020), and then, energized the actuators through the electrodes attached on the both sides of actuators. The frequency of operating signals is chosen as the fundamental frequency of cavity flows. Several operating modes are tested in addition to single-phase mode, here the mode number n is defined as the number of neighboring actuators driven by the same signals. For instance, mode 2 means that the sign of signals becomes opposite between every two neighboring actuators, i.e., 180 degrees out-of-phase, while mode 4 in the unimorph type and mode 8 in the bimorph type are equal to the single-phase mode. Consequently, the possible modes are common divisions of total number of actuators.

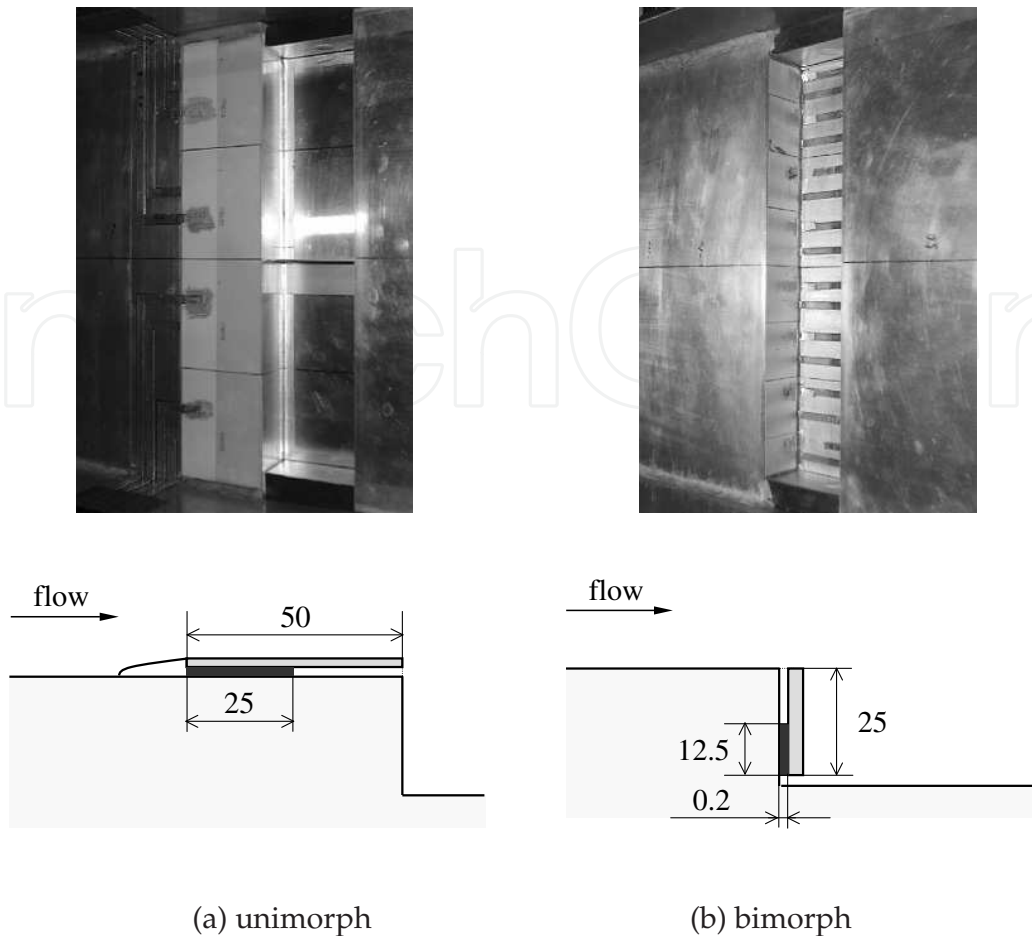


Fig. 3. Piezoelectric actuators.

type	No. of pcs.	mode
unimorph	4	1, 2, 4 (= single-phase)
bimorph	4	1, 2, 4, 8 (=single-phase)

Table 1. Operating modes of actuators.

We use these actuators to control the turbulent-separating cavity flows at $U_\infty = 30\text{m/s}$, where the boundary layer is tripped by a wire ($\phi = 0.5\text{mm}$) together with a piece of sandpaper (No.80) attached to the surface. The thickness of turbulent boundary layer is approximately 7.5mm at the upstream edge of the cavity, 300mm away from the leading edge. Figure 4 shows the FFT spectral analyses of cavity noise and velocity fluctuation inside the shear layer. Both signals have an outstanding peak at around 520Hz. Therefore, this frequency is chosen as the control frequency of actuators. Figures 5 and 6 show the contour map of velocity fluctuations u' in xz plane at $y = 0\text{mm}$ when the supply voltage $V_{\text{rms}} = 70\text{V}$. These graphs are obtained by the ensemble averaging method with the conditional sampling, where the sound signal captured by the microphone is used as the reference signal. The broken lines in the figures indicate the boundaries of the actuators that have the same operating signal. Two-dimensional fluctuation patterns appear along the spanwise direction in the without control case. In particular, these stripe patterns become intense when all actuators are activated by the same operating signal, because the timings of rolling up process are in phase owing to the actuators' motions. The

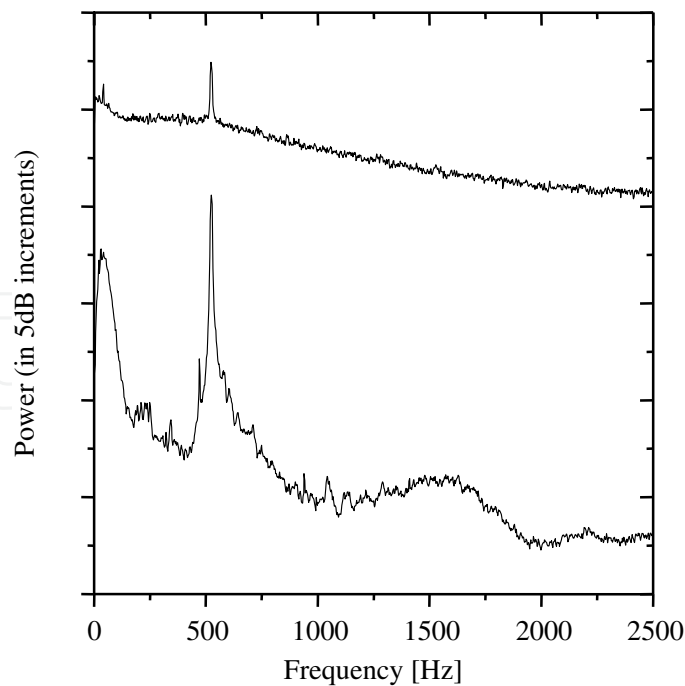


Fig. 4. Power spectra of velocity and pressure fluctuation.

distance between positive and negative stripes is approximately $0.26L \sim 0.28L = 13 \sim 14\text{mm}$. Supposing that the rolled-up vortices travel downstream at the half of the freestream velocity, 15m/s , the frequency of cavity noise can be roughly estimated as $536 \sim 577\text{Hz}$. As shown in Fig. 5, more or less two-dimensional patterns are still observed and no wavy patterns with spanwise phase difference can be found, whether the unimorph-type actuators are activated or not. On the other hand, it is clearly found that the phase of velocity fluctuations is switched from positive to negative or negative to positive at the boundaries of bimorph-type actuators for each operating mode.

Figure 7 presents the noise reduction effects for different supply voltages. The data is plotted as the difference from the peak level of the fundamental frequency around 520Hz without control case, as shown with a dotted line in the figure. The cavity noise increases when all actuators move at the same phase (single-phase), because the two-dimensionality is enhanced by the actuators (see, Fig. 5 (b)). On the other hand, the noise levels go down for each operating mode in both types. It is also found that the bimorph type actuators attached on the upstream sidewall are more effective than the unimorph type actuators (see, Fig. 5 (c), (d) and Fig. 6). Although the unimorph type actuators have the ability to suppress the cavity noise for laminar separating flows, they lose the control effect in the turbulent separating flows since the displacement of actuators becomes relatively smaller in the turbulent boundary layers. Even if the incoming boundary layer is laminar, same problem becomes obvious as the Reynolds number increases.

To obtain the larger displacement, it is necessary to amplify the actuator's displacement in some way. Thus, in this study, we take advantage of the natural frequency of thin aluminum plate, as shown in Fig. 8, where l_1 and w_1 are the length and width of beam 1, l_2 and w_2 the length and width of extra rectangular mass 2. Their thickness h is 1mm . A piece of unimorph actuator, that is 60mm long, 15mm wide and 0.3mm thick, is glued onto the one surface of the T-shaped plate. The actuator is activated at the natural frequency of the T-plate. The frequency can be adjusted by changing the length of the head of the T-plate. Since the

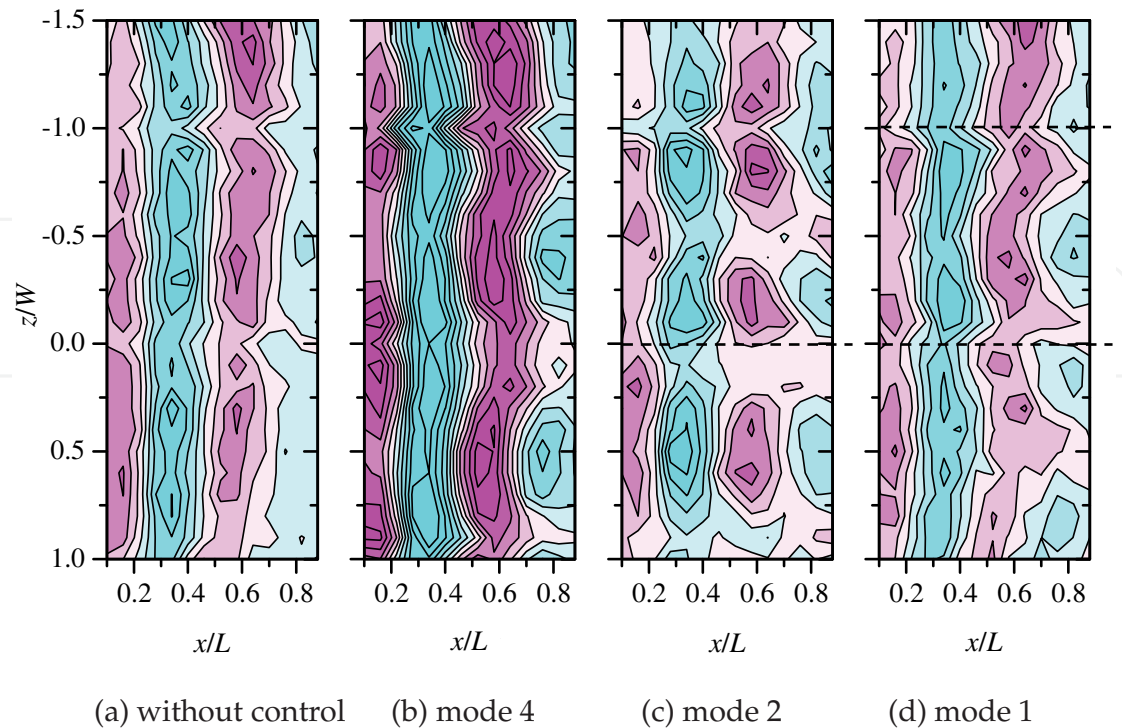


Fig. 5. Contour maps of velocity fluctuations u' in xz plane at $y = 0\text{mm}$, $U_\infty = 30\text{m/s}$ and $V_{\text{rms}} = 70\text{V}$. Contour interval is $0.03U_\infty$. (a) Without control, (b) mode 4 (single-phase), (c) mode 2, (d) mode 1. (Unimorph type)

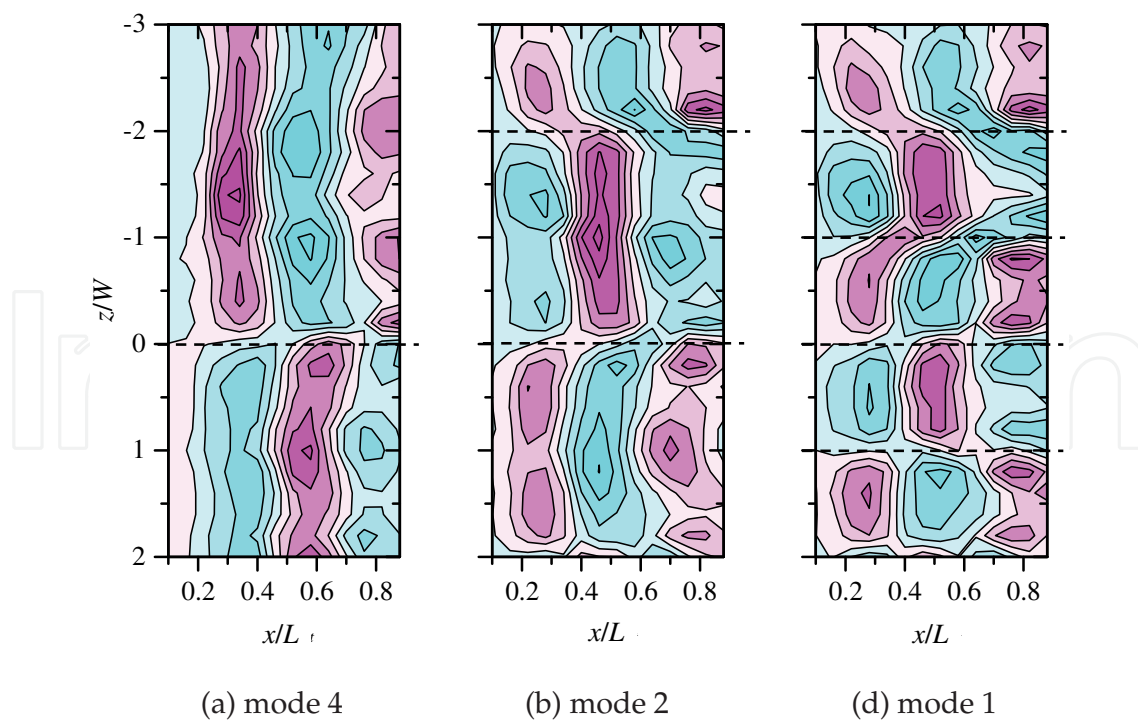
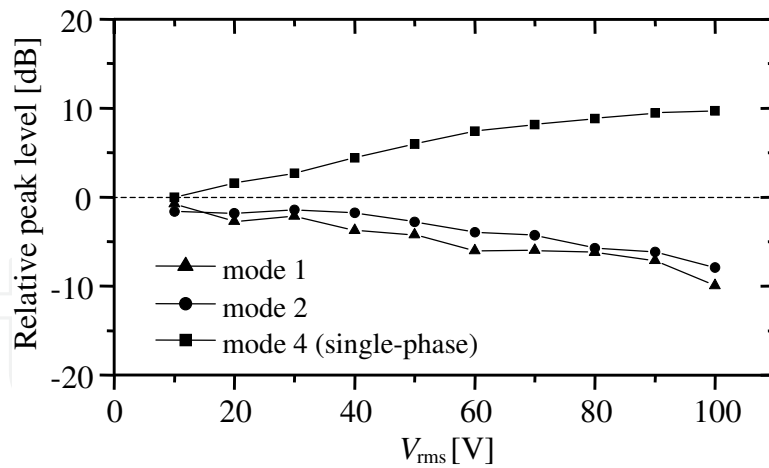
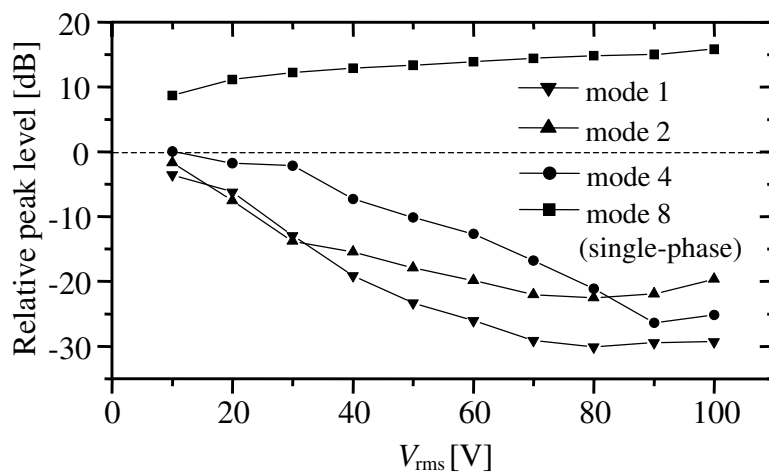


Fig. 6. Contour maps of velocity fluctuations u' in xz plane at $y = 0\text{mm}$, $U_\infty = 30\text{m/s}$ and $V_{\text{rms}} = 70\text{V}$. Contour interval is $0.03U_\infty$. (a) Mode 4, (c) mode 2, (d) mode 1. (Bimorph type)



(a) unimorph type



(b) bimorph type

Fig. 7. Peak level dependence on supply voltage.

bottom of the T-plate is screwed to the wall and fixed, the tip of the plate vibrates back and forth in response to the actuator's expanding and contracting motion. The maximum stroke of the T-plate reaches 1mm, which is hundred times larger than that of an unimorph-type actuator. Twelve such T-plate actuators are set along the spanwise direction 1mm away from the upstream sidewall of the cavity, in a similar way as the bimorph-type actuators.

From the analogy of spring-mass system, the first natural frequency of T-shaped cantilever is written by (Narducci et al., 2007)

$$f = \frac{1}{2\pi} \sqrt{\frac{k + \Delta k}{c_1 m_1 + m_2}} \quad (2)$$

where $c_1 = 0.24$, $k + \Delta k$ is the spring constant after the extra mass m_2 is added, $c_1 m_1$ is the effective mass of the cantilever beam. The spring constant $k + \Delta k$ is given by

$$k + \Delta k = \frac{Eh^3}{4} \frac{w_1 w_2}{l_2^3 w_1 + l_1^3 w_2 + 3l_1^2 l_2 w_2 + 3l_1 l_2^2 w_2} \quad (3)$$

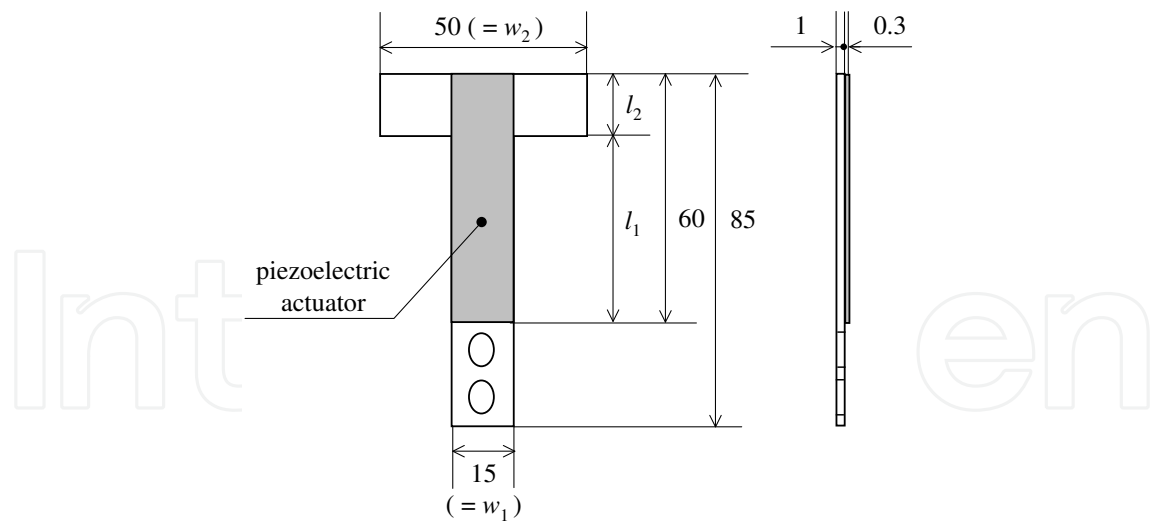


Fig. 8. T-shaped actuator.

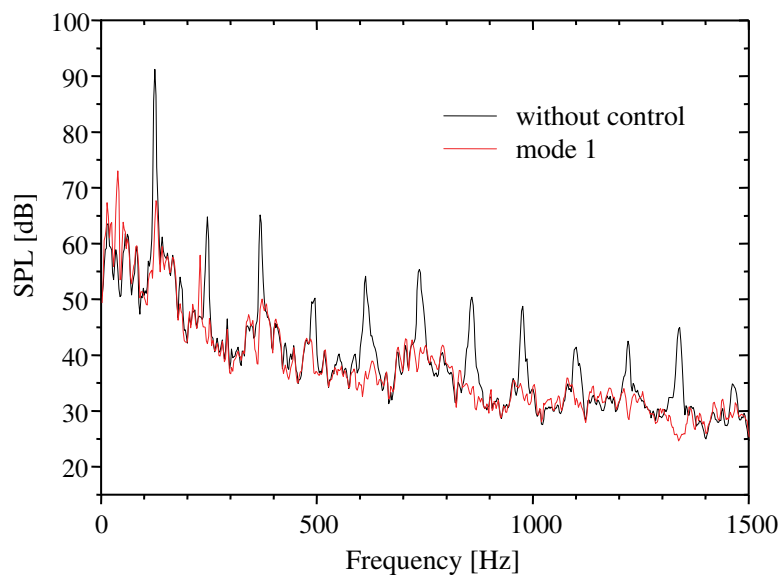


Fig. 9. Noise suppressing effect with the T-shaped actuators at $U_\infty = 21\text{m/s}$.

where E is the Young modulus of the material. For instance, the first natural frequency of the aluminum plate can be estimated to be approximately 112.4Hz for $l_1 = 15\text{mm}$ and 139.5Hz for $l_2 = 8\text{mm}$. However, the actual frequency is expected to be slightly higher than these estimated values, because the piezoelectric actuator is attached. Thus, considering that the target frequency of cavity noise under the current experimental setup is 124.5Hz , we determine the length of extra mass l_1 to be 15mm and the operating frequency of actuators 116Hz .

Figure 9 shows the noise suppression effect of T-shaped actuators when the freestream velocity is 21m/s and the incoming boundary layer is turbulent. The voltage supplied to the actuators is $50V_{\text{rms}}$. As shown the figure, the peak level at 124.5Hz decreases by 23.5dB , and all the higher harmonics components disappear from the spectrum except for the second harmonics. The control effect drops to 17.3dB for larger operating frequency 124Hz ($l_2 = 8\text{mm}$). Thus, the noise suppression effect depends on the operating frequency because the

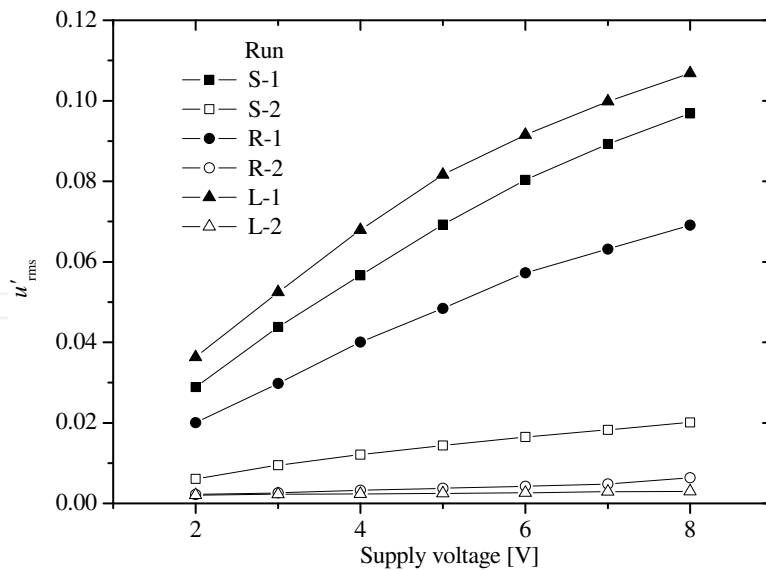


Fig. 11. Variation of the RMS of velocity fluctuation u'_{rms} at $f = 700\text{Hz}$ for different actuator configurations.

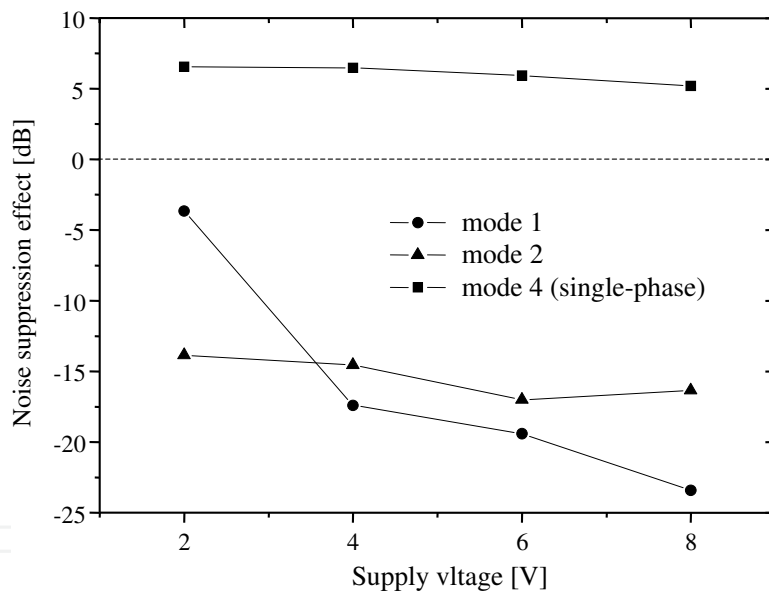


Fig. 12. Noise suppression effects of different operating modes, mode 1, 2 and 4 (single-phase), as a function of the supply voltage at $U_\infty = 25\text{m/s}$. Actuators of $(L_R, L_S) = (\lambda/2, 0)$ are activated at 780Hz .

four conditions can be divided into two groups, whether the actuator is located downstream (Runs R-1 and R-2) or upstream of the slot (Runs L-1 and L-2). Figure 11 plots the velocity fluctuations u'_{rms} for different supply voltages to the loudspeaker. Measurements are carried out in a light wind $U_\infty = 2\text{m/s}$ to keep the sensitivity of hot-wire probe. It is clearly found that the ejection velocity of synthetic actuators depends on their configuration. The velocity fluctuation is proportional to supply voltage for Runs S-1, R-1 and L-1, while it is almost constant at very weak level for Runs S-2, R-2 and L-2 even if the supply voltage is increased.

This is due to the effect of acoustic resonance inside the resonance box otherwise the slot position is not proper. Considering that fluid motion occurs at the opening end not the closing end in a general acoustic-resonance tube, the velocity node equals to the pressure antinode, vice versa. In the current resonator conditions, Comparing the results of Runs R-1 and R-2 or L-1 and L-2, the strong velocity fluctuations are obtained when L_R equals to $\lambda/2$, not to $\lambda/4$. Besides, the results of Runs S-1 and S-2 or L-1 and S-2 indicate that the loudspeaker works as an opening end. In other words, the loudspeaker creates not the fluid motion but the pressure fluctuation. Consequently, we can obtain the strong synthetic jets when the control device satisfies the following two conditions:

Resonance condition : $L_R = \lambda/2 \times n$ ($n = 0, 1, 2, \dots$)

Slot position : Slots should be placed at the velocity node, i.e. the pressure antinode.

And we determine the configuration of synthetic jet actuators as $(L_R, L_S) = (\lambda/2, 0)$.

Figure 12 shows the noise suppression effects of different operating modes, mode 1, 2 and 4 (single-phase), as a function of the supply voltage, where the freestream velocity $U_\infty = 25\text{m/s}$ and the incoming boundary layer is turbulent. The resonance length L_R is determined to 224mm since the target cavity noise has a distinct peak around 780, i.e. $\lambda = 446\text{mm}$, at 88dB that is approximately 38dB larger than the background noise. Vertical axis represents the relative peak levels of cavity noise from that without the control. The cavity noise becomes louder when the all actuators are operated at the same signal (mode 4), while the SPL of the cavity noise goes down for mode 1 and 2 especially for high supply voltage. This means that the synthetic jets are not to strong to blow the shear layer upward never hitting the downstream corner of the cavity, and the noise is suppressed by the superposition of sound sources with 180 degrees out-of-phase.

3.3 Fluidic oscillators

Fluidics is a popular technology that uses the flows and pressures of fluids to control the systems, with no moving parts. The advantage of fluidic-type controllers is that it can introduce much stronger velocity fluctuations than the piezoelectric actuators. Figure 13 shows the schematic of the fluidic-based control device used in this experiment (Shigeta et al., 2008). The behavior of the flow inside the fluidics can be explained as the following: when the airflow supplied by a fan comes into the diffuser section, the Coanda effect makes the flow

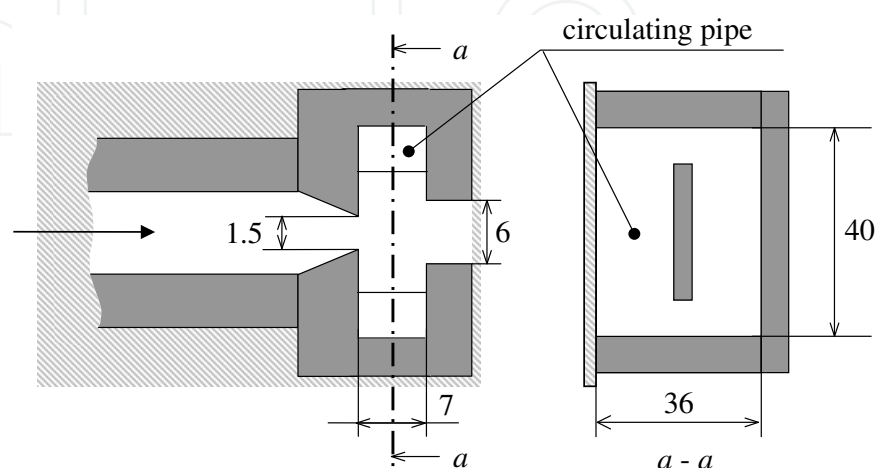


Fig. 13. Schematic of single fluidic oscillator.

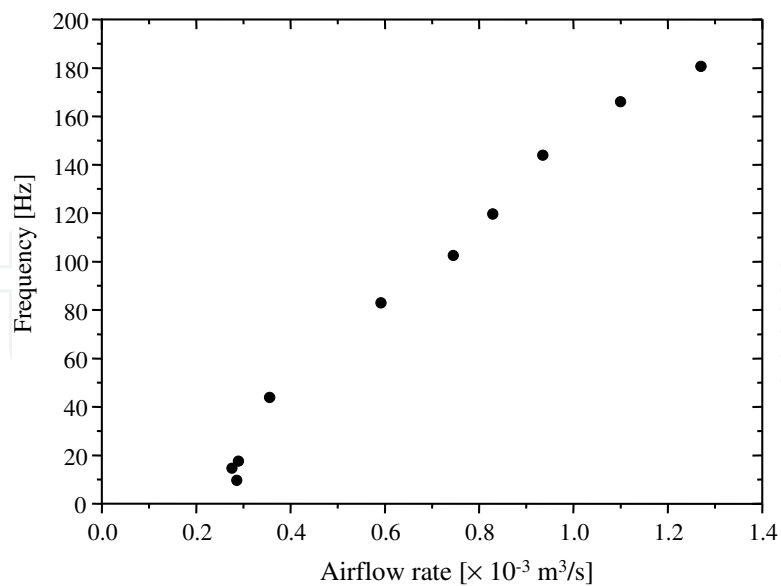


Fig. 14. Variation of oscillating frequency of single fluidic oscillator for different airflow rates.

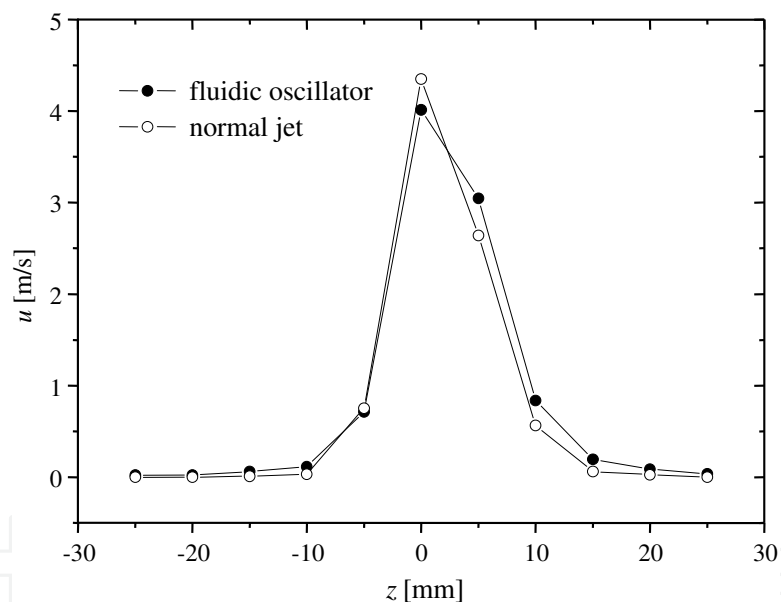


Fig. 15. Mean velocity profiles of oscillating jet and continuous jet.

to blow along one side of the walls. As a result, the difference between the static pressures on both sides arises, which generates a flow through the square pipe. The flow through the circulating pipe then pushes the jet at the other end changing the direction of the jet at the diffuser inlet. This process is successively repeated at a constant frequency. Owing to this self-oscillatory nature of fluidics, self-sustained intermittent jets of a certain frequency are generated. We installed this fluidic oscillator at the center of upstream sidewall of the cavity and 20mm below the upstream surface. Thus, the jet issues from a slot of length 20mm and width 1mm.

The relation between an oscillating frequency and an airflow rate for single fluidic oscillator shown in Fig. 13 is plotted in Fig. 14. The jet frequency increases almost linearly with the

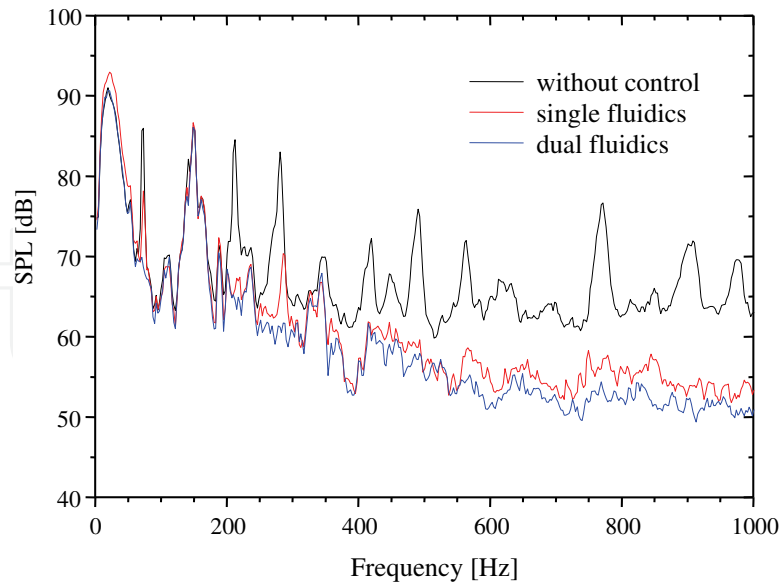


Fig. 16. Noise suppression effect at $U_{\infty} = 23.3\text{m/s}$.

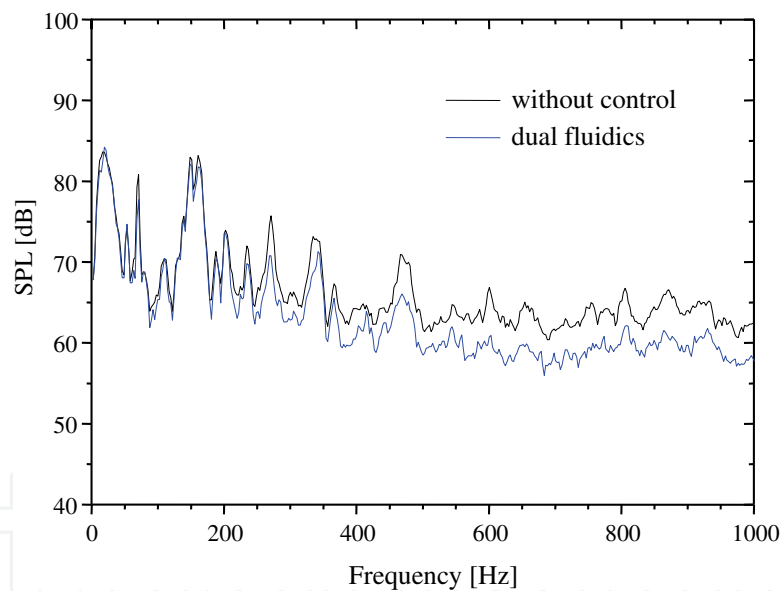


Fig. 17. Noise suppression effect at $U_{\infty} = 26.1\text{m/s}$.

airflow rate from the fan. This characteristic implies the feasibility of controlling the frequency by changing the airflow rate. It should be noted that if one use the multiple fluidic oscillators, it is necessary to synchronize their oscillating phases in some way. Figure 15 shows the mean velocity profiles of oscillating jet and continuous jet issuing from a simple diffuser without a recirculating pipe. The velocity is measured at the slot exit, and the airflow rate is $0.55 \times 10^{-3} \text{ m}^3/\text{s}$. Almost identical distributions can be found. The half width is approximately 10mm, and the maximum velocity exceeds 4m/s. However, the flow velocity is not too high as to change the trajectory of shear layer by pushing it upward.

Figure 16 represents the acoustic spectra with and without control, where the frequency of fluidic oscillators are adjusted to that of the cavity noise. The freestream velocity U_∞ is 23.3m/s and the upstream boundary layer is turbulent. The size of the cavity is 150mm long ($= L$) and 90mm deep ($= D$). A resonator is used to simulate a deep cavity environment because the peaky noise is not generated in the shallow cavity when the flow before separation is turbulent. From the figure, it can be found that the strong peak at 75Hz and its harmonics appearing in the spectrum before control become weaker or disappear after the control which uses the single-fluidic system. However, the peak level of the fundamental frequency is suppressed by only 9dB that corresponds to 47% noise suppression relative to the background noise level. This noise suppressing effect is considerably lower compared to the laminar separating flow case. Hence, we introduced one more fluidic oscillator to enhance the flow controlling effect. The oscillations of the two fluidic controllers are synchronized by connecting each recirculating pipe. The blue line in the figure presents the result of the dual-fluidic system. Compared with the single-fluidic case, the noise suppression effect is much improved by adding the second fluidic oscillator. The cavity noise, including higher harmonic components, disappears from the spectrum. However it drops again to a lower value for higher Reynolds numbers ($U_\infty = 26.1\text{m/s}$), as shown in Fig. 17. These results indicate that more fluidic oscillators are required for controlling the flows of even higher Reynolds numbers. Besides, we also investigated the effect of the continuous jet on the cavity noise for laminar separating flows and the results were compared with the single-fluidic case. As a result, we found that the control effect of the single-fluidic system is superior to that of the continuous jet, even though their time-averaged velocity profiles are nearly equal. This means that the periodical oscillation of jet plays a dominant role in controlling the cavity flows under the current experimental conditions.

4. Passive control

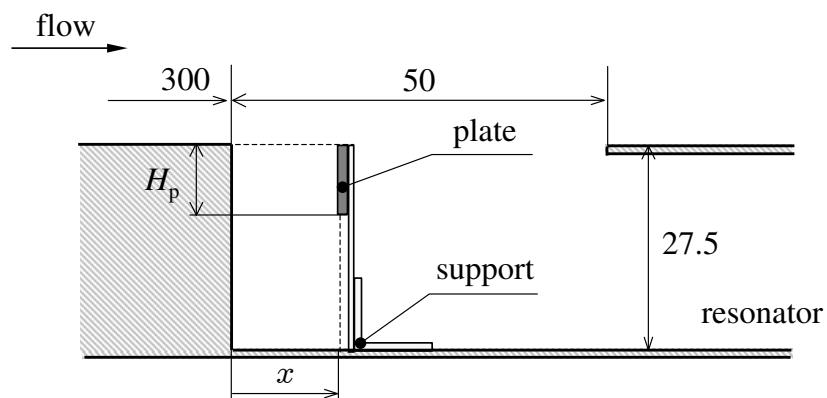
The key point of above active control methods is to control the cavity flows by changing only the timing of vortex rolling up using less energy. Flow receptivity enables this phase-based control. Since the velocity disturbances are added into a boundary layer at the upstream edge of the cavity before the vortex formation, these active control methods can be interpreted as a kind of vaccine against the cavity noise. On the other hand, passive controls usually work on the rolled-up vortices directly. Thus, they have the side of symptomatic treatment. In this study, passive control has also been attempted using a small thin plate and small blockage inserted into a cavity. In the following sections, we discuss the effect of the size and location of the obstacle on the noise suppression, where the obstacle is directly inserted inside the shear layer or just settled on the bottom of the cavity. These studies were started when we happened to notice that the target cavity noise vanished before activating the actuators, during the active control experiments.

4.1 Static plate

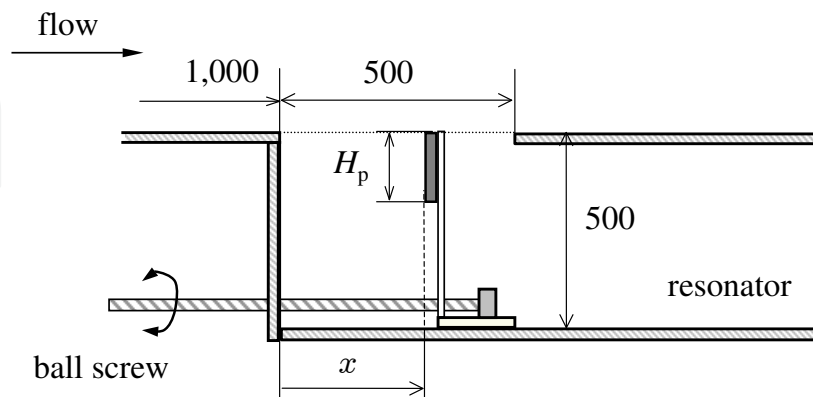
First of all, we describe the effect of a thin two-dimensional plate as a static controlling device to suppress the cavity noise when it is inserted vertically into a cavity (Kuroda et al., 2003; Izawa et al., 2006 & 2007). The experiments were conducted using two different-size wind tunnels: the conventional wind tunnel at IFS in Tohoku University and the large-scale, low-noise wind tunnel of the Railway Technical Research Institute (RTRI). The latter wind tunnel has a rectangular cross-section nozzle of 3m in width and 2.5m in height, and the

turbulence levels of freestream at the test section are about 0.4% at 60m/s. Both results are compared and the effect of scale difference on the noise suppression is also discussed.

Figure 18 shows the cavity models used in each wind tunnel experiment. The geometry of the model is basically the same as that used in the active control experiments, shown in Fig. 2, but the streamwise length of the rectangular cavity L of the RTRI model is ten times as long as that of the IFS model. The model is mounted in the freestream for the IFS experiment, while it is installed so that its leading edge is smoothly connected to the lower side floor of the nozzle for the RTRI experiment. Upstream boundary layer is turned into turbulent by a combination of trip wire ($\phi = 0.5\text{mm}$) and sandpaper (No. 400) for the IFS tunnel, or a trip wire ($\phi = 1.5\text{mm}$) for the RTRI tunnel. The length of a resonator is adjusted to according to the frequency of the cavity noise. A flow-controlling plate with various lengths H_p in the y direction is placed inside the cavity. The plate is fixed on the floor by L-shape supports. For convenience, we designed that the streamwise plate position can be easily changed using a ball screw without turning off the wind tunnel during the RTRI experiment. It should be noted that the RTRI model is made strong enough by a combination of 16mm thick wooden fat plates and aluminum frames, since the plate surface is exposed to the strong negative pressure of the freestream. The freestream velocity U_∞ is set at 30m/s for the IFS tunnel and



(a) cavity mode at IFS



(b) cavity model at RTRI

Fig. 18. Schematic of the cavity models used at (a) IFS and (b) RTRI.

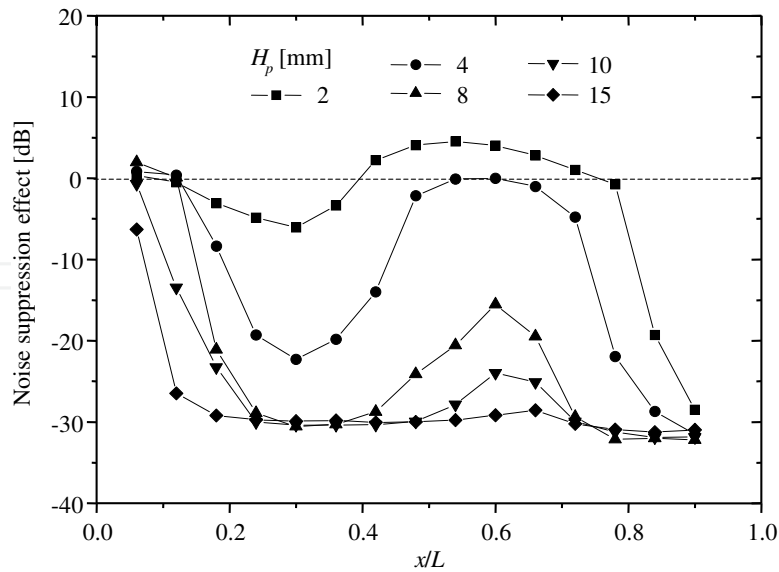


Fig. 19. Variation of peak level with different plate height H_p and streamwise locations x at IFS.

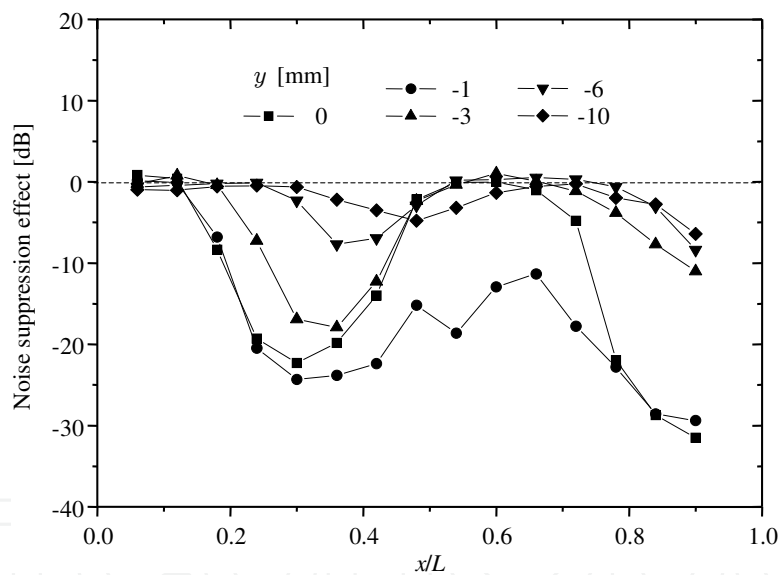
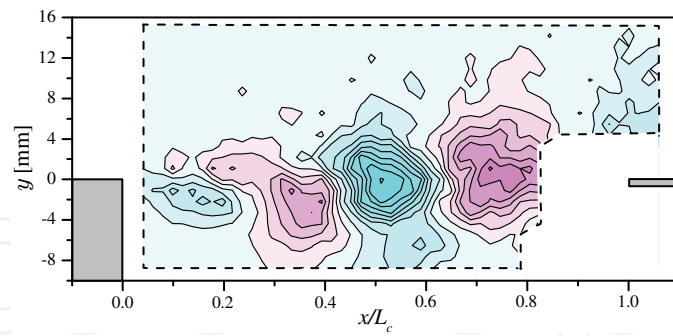


Fig. 20. Variation of peak level with different wall-normal locations y for $H_p = 4$ mm at IFS.

60m/s for the RTRI tunnel, where the thickness of turbulent boundary layer at the upstream edge of the cavity is approximately 11mm and 104mm, respectively.

Variation of noise suppression effect for various plate height H_p and positions (x, y) for the IFS experiment is shown in Figs. 19 and 20. The frequency of the cavity noise is 480Hz and the resonator length is set at 140mm. The peak level of the cavity noise strongly depends on the plate location, not only the streamwise but also the wall-normal directions. In particular, the noise suppression effect becomes obvious at two streamwise positions, around $x/L = 0.3$ and near the downstream edge of the cavity. Besides, the effect is gradually saturated except for the region near the upstream and downstream edges with the increase in the vertical length of



(a) without plate

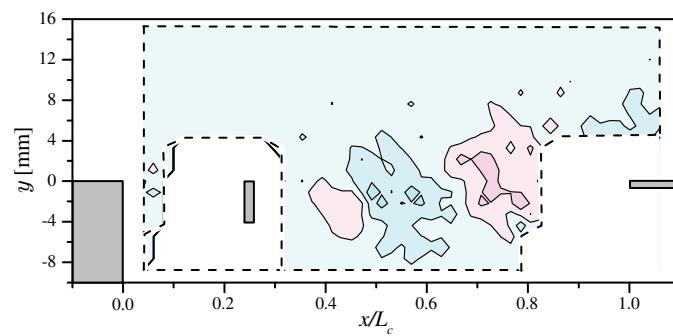
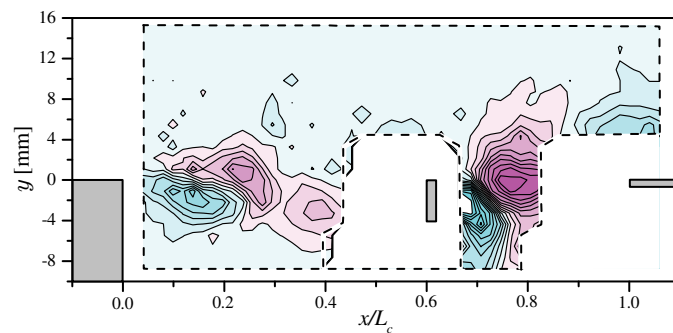
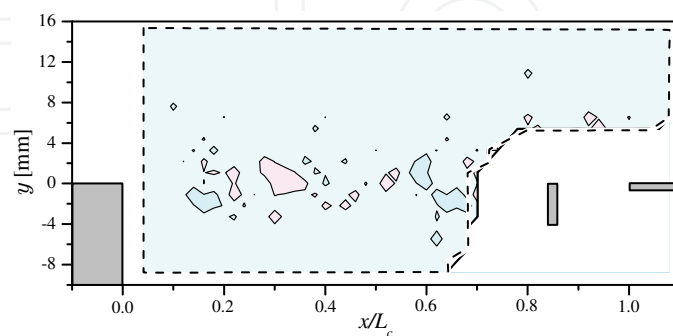
(b) plate at $x/L = 0.24$ (c) plate at $x/L = 0.6$ (d) plate at $x/L = 0.84$

Fig. 21. Contour maps of spanwise vorticity fluctuation ω'_z without plate (a) with plate at $x/L = 0.24$ (b), 0.6 (c) and 0.84 (d). Contour interval is 0.66 . ($H_p = 4\text{mm}$ and $y = 0\text{mm}$, IFS)

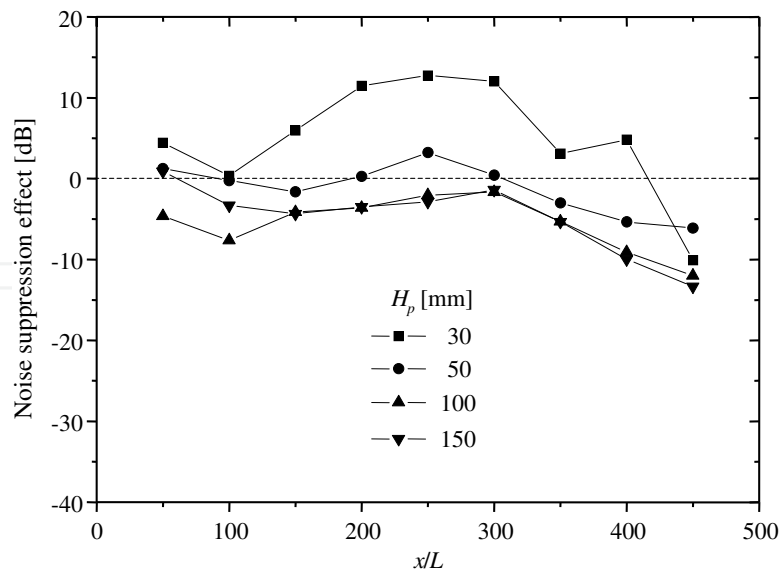


Fig. 22. Variation of peak level with different plate height H_p and streamwise locations x at RTRI.

the plate. The maximum value of noise reduction reaches approximately 30dB that is nearly equivalent to the amount amplified by the existence of the resonator. These facts imply that the resonance inside the cavity may be damaged by a large plate covering the cavity. It is also found that the noise reduction effect is lost when the plate is lower than $y = -6\text{mm}$, which is the outer edge of the shear layer. On the other hand, the effect suddenly drops near the downstream edge, when the plate position is changed from $y = -1\text{mm}$ to -3mm . This implies that the noise suppression mechanism is different in the two cases.

Figure 21 shows the contour maps of the spanwise vorticity fluctuation measured by X-type hot-wire probe when the plate of $H_p = 4\text{mm}$ is placed at various streamwise positions, $y = 0\text{mm}$. The strong pattern causing the intense cavity noise becomes weaker or disappears at $x/L = 0.24$ and 0.84 . The upstream plate directly discourages the rolling-up process of the shear layer, while the downstream plate weakens the feedback loop by easing the pressure fluctuation generated by the periodical impingement of rolled-up vortices into the downstream corner of the cavity. Besides, considering that the vortices hit the corner at $y = -3 \sim 2.5\text{mm}$, the plate whose position is lower than $y = -3\text{mm}$ has no influence on the vortices. This is the reason of the rapid decrease in the control effect of the plate at $y = -3\text{mm}$ near the downstream edge, shown in Fig. 20. When the plate is placed at $x/L = 0.6$, no obvious effect is also observed because the vertical size of the plate H_p is so small compared to the thickness of the shear layer that the rolled-up vortices cannot be destroyed by the plate.

The noise suppression effect at the large wind tunnel of RTRI is plotted in Fig. 22. The frequency of the cavity noise is 89Hz and the resonator length is determined to be 800mm from the preliminary experiment. As well as the small wind tunnel experiment at IFS, after the SPL decreases at $x/L = 0.2 \sim 0.3$, it increases near the center of the cavity and decreases again as the plate becomes closer to the downstream edge. The maximum effect is obtained when H_p is equal to the thickness of the shear layer. However, the noise suppression effect is smaller compared to the IFS experiment, since the noise generation of the plate itself cannot be ignored in such a high-speed flows.

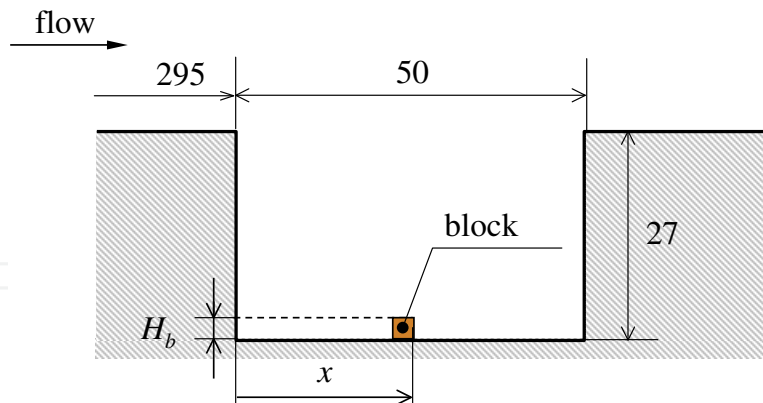


Fig. 23. Schematic of static block placed on the floor of a cavity.

4.2 Small block on the floor

When a shear layer passes a cavity, it mainly keeps flowing downstream but the rest comes into the cavity and forms a recirculating flows. In this section, we discuss the feasibility of suppressing the cavity noise generation by controlling the recirculating fluid motions inside a rectangular cavity without a resonator (Izawa et al., 2010). Figure 23 shows the schematic of static block inserted on the floor of a cavity of 50mm in length and 27mm in depth. A block has a square cross section, H_b mm on a side, and its noise suppression effect is investigated by changing the size and position. The freestream velocity is constant at $U_\infty = 18\text{m/s}$ and the target flow is laminar. At the upstream edge of the cavity, the laminar boundary thickness is approximately 2.6mm.

Figure 24 present the spectra of the cavity noise with and without a block of $H_b = 2\text{mm}$ that is placed at the center of the cavity, $x/L = 0.5$. The dominant peak at 820Hz shown in the original spectrum completely disappears owing to the small block on the floor. Both sound signals are analyzed using a wavelet transform and the results are compared. Figure 25 shows the wavelet spectra of both signals. When there is no block, an intense streak is clearly observed independently in time around the fundamental frequency of the cavity noise, 820Hz. It is interesting that when the block is installed, the streak pattern becomes intermittently but still left in the spectrum, though the corresponding peak cannot be seen in the FFT spectrum shown in Fig. 24. This means that the continuous feedback loop is destroyed but it still alive on and off. Variation of effective size and position of the block is plotted in Fig. 26. The solid lines connecting two dot points in the figure represent the regions where the SPL of the cavity noise decreases to the background noise level. The optimum block position shifts toward the upstream side of the cavity, as the block size H_b increases. Besides, it is also found that the optimum position moves downstream for longer cavity, $L/D = 2$.

5. Conclusion

We have successfully suppressed the cavity noise for through both the active and passive control approaches at low Mach numbers ($M \leq 0.18$). Active control is achieved with the use of piezoelectric actuators, synthetic jets and fluidic oscillators. These actuators are attached on the upstream wall of a cavity side by side, for the purpose of adding weak periodic velocity fluctuations to the shear layer. Their operating frequency is chosen to be the natural frequency of the shear layer and only the timing of the separation at the leading edge is controlled in the spanwise direction. Thanks to flow receptivity, resulting pressure fluctuations hence

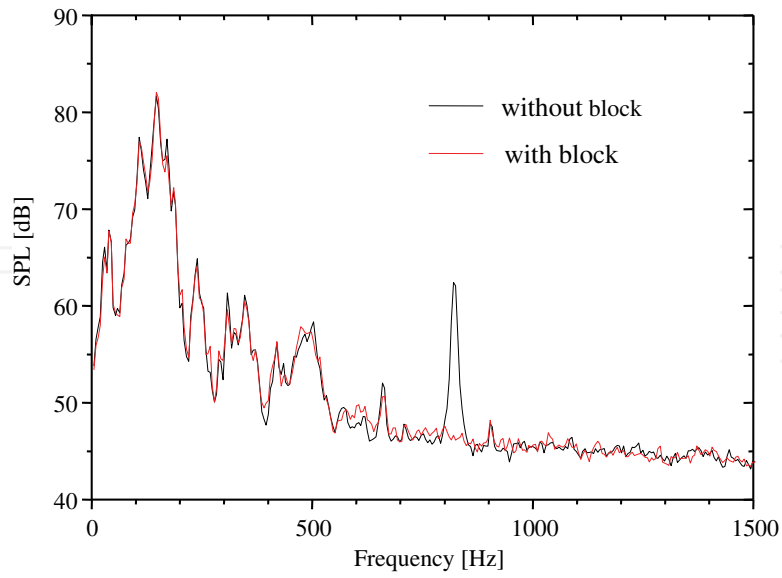


Fig. 24. SPL of cavity noise with and without a block of $H_b = 2\text{mm}$ at $x/L = 0.5$.

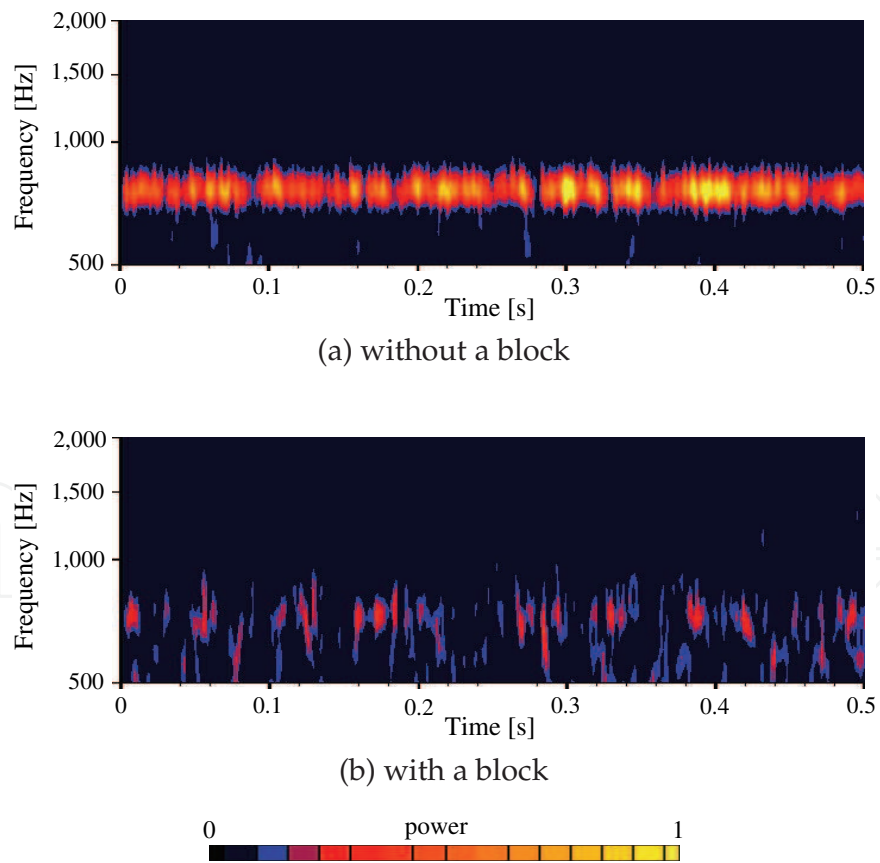


Fig. 25. Wavelet spectra (a) without and (b) with a square block of $H_b = 2\text{mm}$ at $x/L = 0.5$.

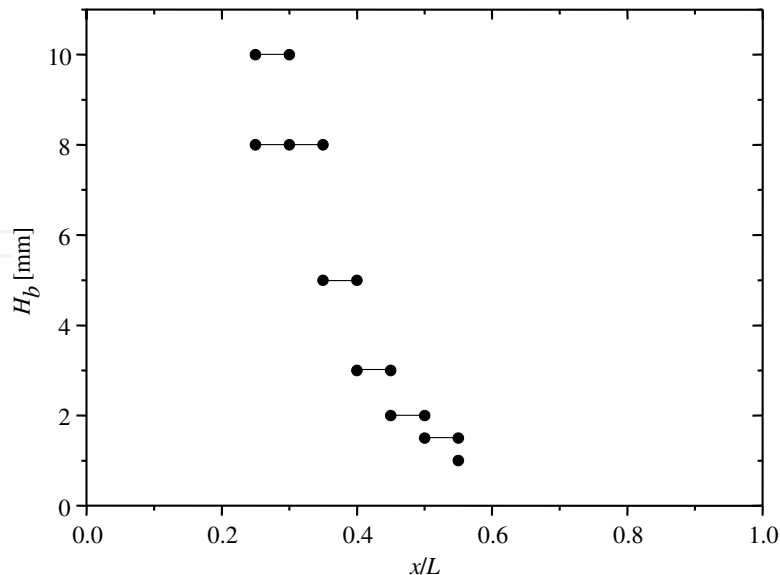


Fig. 26. Effective sizes and positions of the plate for noise suppression. Solid lines represent the positions where the cavity noise completely disappears.

the sound waves coming out become 180 degrees out of phase, and consequently, these opposite-signed sound waves cancel each other faraway from the cavity, though the noise generation itself is not reduced at the source. In addition to active control, passive control experiments are also performed using a small thin plate and small block inserted into the cavity.

The phase control method at the upstream edge of the cavity is capable of effectively suppressing the noise, while the thin plate inserted inside the shear layer also shows large noise suppression effect when it is placed near the upstream edge or the downstream edge. Besides, the cavity noise can be suppressed by a small block placed at the bottom surface, which is inserted in the middle of the cavity. However, the sound suppression efficiency has limitations depending on the scale of the flow field, because the magnitude of the velocity fluctuations introduced by the actuators becomes relatively smaller owing to the limitation in the size and power of the piezoelectric device, and the noise generated from the plate itself cannot be neglected in large-scale experiments, cutting down the noise suppression effect.

6. Acknowledgments

Forepart of this work was supported by the Grant-in-Aid for Scientific Research (A)#11355009, Japan Society for Promotion of Science. The support of the Railway Technical Research Institute (RTRI) is also greatly acknowledged. The series of these experiments have been performed by our former graduate students as research projects for their Ph.D. and master theses. The author wishes to thank all of them, Yuzuru Yokokawa, Masafumi Kuroda, Hiroshi Maita, Katsuo Kobayashi, Shota Maehara, Toshimasa Miura, Ryuzo Sakamoto, Hiroaki Nishida, Hiroyuki Nakashima, and my colleagues Prof. Fukunishi and Asst. Prof. Shigeta.

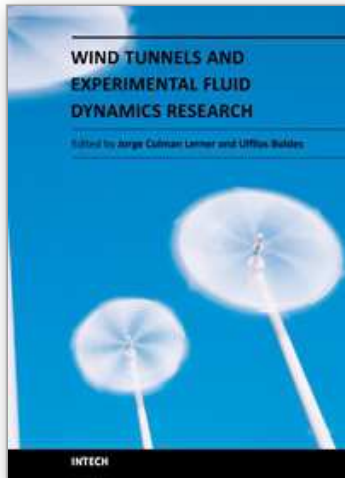
7. References

- Asai, T. & Nishioka, M. (2003). An Experimental Study on the Mechanism of Supersonic Cavity Flow Oscillations, *Journal of Japan Society of Fluid Mechanics* Vol. 22 (No. 2), 131-145 (in Japanese).
- Cattafesta III, L.N., Song, Q., Williams, D.R., Rowley, C.W. & Alvi, S.F. (2008). Active control of flow-induced cavity oscillations, *Progress in Aerospace Sciences* Vol. 44, 479-502.
- Chang, K., Constantinescu, G. & Park, S.-O. (2006). Analysis of the flow and mass transfer processes for the incompressible flow past an open cavity with a laminar and a fully turbulent incoming boundary layer, *Journal of Fluid Mechanics* Vol. 561, 113-145.
- Chicheportiche, J. & Gloerfelt, X. (2010). Direct noise computation of the flow over cylindrical cavities, *AIAA Paper* 2010-3775, 1-12.
- De Roeck, W., Rubio, G., Baelmans, M. & Desmet, W. (2009). Toward accurate hybrid prediction techniques for cavity flow noise applications, *International Journal for Numerical Methods in Fluids* Vol. 61, 1363-1387.
- Faure, T.M., Adrianos, P., Lusseyan, F. & Pastur, L. (2006). Visualization of the flow inside an open cavity at medium range Reynolds numbers, *Experiments in Fluids* Vol. 42 (No. 2), 169-184.
- Fukunishi, Y., Yokokawa, Y. & Izawa, S. (2002). ACTIVE CONTROL OF TURBULENT SEPARATING FLOW OVER A CAVITY FOR NOISE SUPPRESSION, *Proceedings of the Ninth Asian Congress of Fluid Mechanics*, ACFM9, 1-6.
- Gloerfelt, X., Bailly, C. & Juvé, D. (2003). Direct computation of the noise radiated by a subsonic cavity flow and application of integral methods, *Journal of Sound and Vibration* Vol. 266, 119-146.
- Gloerfelt, X. (2009). Noise from automotive components, *Aerodynamic noise from wall-bounded flows*, coll. VKI Lectures, March 9-13.
- Grace, S.M. (2001). AN OVERVIEW OF COMPUTATIONAL AEROACOUSTIC TECHNIQUES APPLIED TO CAVITY NOISE PREDICTION, *AIAA Paper* 2001-0510, 1-13.
- Heller, H.H., Holmes, D.G. & Covert, E.E. (1971). FLOW-INDUCED PRESSURE OSCILLATIONS IN SHALLOW CAVITIES, *Journal of Sound and Vibration* Vol.18 (No. 4), 545-553.
- Hémmon, P., Amandolése, X., Santi, F. & Wojciechowski, J. (2002). STUDY OF THE ACOUSTIC OSCILLATION OF FLOW OVER CAVITIES. PART 2. SOUND REDUCTION, *Proceedings of IMECE2002 ASME International Mechanical Engineering Conference & Exposition*, IMCE2002-33376, 1-7.
- Huang, X. & Zhang, X. (2008). Streamwise and spanwise plasma actuators for flow-induced cavity noise control, *Physics of Fluids* Vol. 20 (No. 3), 1-10.
- Izawa, S., H. Maita, Terashima, O., Xiong, A.K. & Fukunishi, Y. (2006). Sound Suppression of Laminar Separating Flow Over Cavity, *JSME International Series B* Vol.49 (No.4), 1092-1097.
- Izawa, S., Kuroda, M., Ido, A. & Fukunishi, Y. (2007). Effect of Static Control Device on Suppression of Cavity Noise, *Journal of Environmental and Engineering* Vol.2 (No.1), 194-202.
- Izawa, S., Nishida, H., Shigeta, M. & Fukunishi, Y. (2010). SUPPRESSION OF AERODYNAMIC NOISE GENERATION BY CONTROLLING THE CIRCULATING FLUID MOTION INSIDE A CAVITY, *Proceedings of the International Conference on Jet, Wakes and Separated Flows ICJWSF-2010*, 1-3.

- Kegerise, K.A., Cattafesta, L.N. & Ha, C. (2002). Adaptive Identification and Control of Flow-Induced Cavity Oscillations, *AIAA Paper* 2002-3158, 1-10.
- Kim, C.-K., John Yu, S.-T. & Zhang, Z.-C. (2004). Cavity Flow in Scramjet Engine by Space-Time Conservation and Solution Element Method, *AIAA Journal* Vol. 42 (No. 5), 912-919.
- Kuo, C.H. & Chang, C.W. (1998). Shear-layer characteristics across a cavity with a horizontal top plate, *Fluid Dynamic Research* Vol. 22, 89-104.
- Kuo, C.H. & Huang, S.H. (2001). Influence of flow path modification on oscillation of cavity shear layer, *Experiments in Fluids* Vol. 31, 162-178.
- Kuo, C.H. & Huang, S.H. (2003). Effect of surface mounting of upper plate on oscillating flow structure within cavity, *Experimental Thermal and Fluid Science* Vol. 27, 755-768.
- Kuroda, M., Izawa, S., Xiong, A.K. & Fukunishi, Y. (2003). SUPPRESSION OF AERO-ACOUSTIC NOISE OVER A CAVITY, *Proceedings of the 4th ASME/JSME Joint Fluid Engineering Conferences*, FEDSM2003-45194, 1-6.
- Larchevêque, L., Sagaut, P. & Labbe O. (2007). Large-eddy simulation of a subsonic cavity flow including asymmetric three-dimensional effects, *Journal of Fluid Mechanics* Vol. 577, 105-126.
- MacManus, D.G. & Doran, D.S. (2008). Passive Control of Transonic Cavity, *Journal of Fluids Engineering* Vol. 130 (No. 6): 1-4.
- Marsden, O., Jondean, E., Souchotte, P., Bogey, C., Bailly, C. & Juvé, D. (2008). Investigation of flow features and acoustic radiation of a round cavity, *AIAA Paper* 2008-2851, 1-13.
- Micheau, P., Chatellier, L., Laumonier, J. & Gervais, Y. (2005). Stability analysis of active control of self-sustained pressure fluctuations due to flow over cavity, *Journal of Acoustic Society of America* Vol. 119 (No. 3), 1496-1503.
- Narducci, M., Figueras, E., Gràcia, I., Fonseca, L. Santander, J. & Cané, C. (2007). MODELING OF T-SHAPED MICROCANTILEVER RESONATORS, *Proceeding of the Symposium on Design, Test, Integration and Package of MEMS / MOEMS*, DTIP2007, 100-105.
- Nishioka, M., Asai, T., Sakaue, S. & Shirai, K. (2002). Some Thoughts on the Mechanism of supersonic Cavity Flow Oscillations. Part 1. Generation and Propagation Processes of Compression Waves, *Journal of Japan Society of Fluid Mechanics* Vol. 21 (No. 3), 280-294.
- Raman, G., Raghu, S. & Bencic, T.J. (1999). Cavity Resonance Suppression Using Miniature Fluidic Oscillators, *AIAA Paper* 99-1900, 1-22.
- Rockwell, D. & Knisely, D. (1979). The organized nature of flow impingement upon a corner, *Journal of Fluid Mechanics* Vol. 93, 413-432.
- Rossiter, J.E. (1964). Wind-Tunnel Experiments on the Flow over Rectangular Cavities at Subsonic and Transonic Speeds, *Aeronautical Research Council Reports and Memoranda* No. 3438.
- Rowley, C.W. & Williams, D.R. (2003), CONTROL OF FORCED AND SELF-SUSTAINED OSCILLATIONS IN THE FLOW PAST A CAVITY, *AIAA Paper* 2003-0008, 1-8.
- Rowley, C.W., Juttijudata, V. & Williams, D.R. (2005). Cavity Flow Control Simulations and Experiments, *AIAA Paper* 2005-02592, 1-11.
- Shigeta, M., Miura, T., Izawa, S. & Fukunishi, Y. (2008). Active Control of Cavity Noise by Fluidic Oscillators, *Theoretical and Applied Mechanics* Vol. 57, 127-134.
- Williams, D.R. & Rowley, C.W. (2006). Recent Progress in Closed-Loop Control of Cavity Tones, *AIAA Paper* 2006-0712, 1-12.

- Yokokawa, Y., Fukunishi, Y. & Kikuchi, S. (2000). SUPPRESSION OF AERO-ACOUSTIC NOISE BY SEPARATION CONTROL USING PIEZO-ACTUATORS, *AIAA Paper* 2000-1931, 1-9.
- Yokokawa, Y. & Fukunishi, Y. (2001). Reduction of Aerodynamic Noise Generation at the Cavity by Active Flow Control Using Thin Ceramic Actuator Pieces, *Theoretical and Applied Mechanics* Vol. 50, 281-287.
- Yokoyama, H. & Kato, C. (2009). Fluid-acoustic interactions in self-sustained oscillations in turbulent cavity flows. I. Fluid-dynamic oscillations, *Physics of Fluids* Vol. 21 (No. 10), 1-13.
- Yoshida, T., Watanabe, T., Ikeda, T. & Ito, S. (2006). Numerical Analysis of Control of Flow Oscillations in Open Cavity Using Moving Bottom Wall, *JSME International Journal Series B* Vol. 49 (No. 4), 1098-1104.

IntechOpen



Wind Tunnels and Experimental Fluid Dynamics Research

Edited by Prof. Jorge Colman Lerner

ISBN 978-953-307-623-2

Hard cover, 709 pages

Publisher InTech

Published online 27, July, 2011

Published in print edition July, 2011

The book "Wind Tunnels and Experimental Fluid Dynamics Research" is comprised of 33 chapters divided in five sections. The first 12 chapters discuss wind tunnel facilities and experiments in incompressible flow, while the next seven chapters deal with building dynamics, flow control and fluid mechanics. Third section of the book is dedicated to chapters discussing aerodynamic field measurements and real full scale analysis (chapters 20-22). Chapters in the last two sections deal with turbulent structure analysis (chapters 23-25) and wind tunnels in compressible flow (chapters 26-33). Contributions from a large number of international experts make this publication a highly valuable resource in wind tunnels and fluid dynamics field of research.

How to reference

In order to correctly reference this scholarly work, feel free to copy and paste the following:

Seiichiro Izawa (2011). Active and Passive Control of Flow Past a Cavity, Wind Tunnels and Experimental Fluid Dynamics Research, Prof. Jorge Colman Lerner (Ed.), ISBN: 978-953-307-623-2, InTech, Available from: <http://www.intechopen.com/books/wind-tunnels-and-experimental-fluid-dynamics-research/active-and-passive-control-of-flow-past-a-cavity>

INTECH
open science | open minds

InTech Europe

University Campus STeP Ri
Slavka Krautzeka 83/A
51000 Rijeka, Croatia
Phone: +385 (51) 770 447
Fax: +385 (51) 686 166
www.intechopen.com

InTech China

Unit 405, Office Block, Hotel Equatorial Shanghai
No.65, Yan An Road (West), Shanghai, 200040, China
中国上海市延安西路65号上海国际贵都大饭店办公楼405单元
Phone: +86-21-62489820
Fax: +86-21-62489821

© 2011 The Author(s). Licensee IntechOpen. This chapter is distributed under the terms of the [Creative Commons Attribution-NonCommercial-ShareAlike-3.0 License](#), which permits use, distribution and reproduction for non-commercial purposes, provided the original is properly cited and derivative works building on this content are distributed under the same license.

IntechOpen

IntechOpen